Published in final edited form as:
J Biomech. 2021 March 30; 118: 110279. doi:10.1016/j.jbiomech.2021.110279.

Focused targeting of inhaled magnetic aerosols in reconstructed *in vitro* airway models

Yan Ostrovski[a], **Semion Dorfman**[a], **Wilson Poh**[b], **Say Chye Joachim Loo**[b,c], **Josué Sznitman**[a,*]

[a]Department of Biomedical Engineering, Technion – Israel Institute of Technology, Haifa, Israel

[b]School of Material Science and Engineering, Nanyang Technological University, Singapore

[c]Singapore Centre for Environmental Life Sciences Engineering (SCELSE), Nanyang Technological University, Singapore

Abstract

The pulmonary tract is an attractive route for topical treatments of lung diseases. Yet, our ability to confine the deposition of inhalation aerosols to specific lung regions, or local airways, remains still widely beyond reach. It has been hypothesized that by coupling magnetic particles to inhaled therapeutics the ability to locally target airway sites can be substantially improved. Although the underlying principle has shown promise in seminal *in vivo* animal experiments as well as *in vitro* and *in silico* studies, its practical implementation has come short of delivering efficient localized airway targeting. Here, we demonstrate in an *in vitro* proof-of-concept an inhalation framework to leverage magnetically-loaded aerosols for airway targeting in the presence of an external magnetic field. By coupling the delivery of a short pulsed bolus of sub-micron (~500 nm diameter) droplet aerosols with a custom ventilation machine that tracks the volume of air inhaled past the bolus, focused targeting can be maximized during a breath hold maneuver. Specifically, we visualize the motion of the pulsed SPION-laden (super-paramagnetic iron oxide nanoparticles) aerosol bolus and quantify under microscopy ensuing deposition patterns in reconstructed 3D airway models. Our aerosol inhalation platform allows for the first time to deposit inhaled particles to specific airway sites while minimizing undesired deposition across the remaining airspace, in an effort to significantly augment the targeting efficiency (i.e. *deposition ratio* between targeted and untargeted regions). Such inhalation strategy may pave the way for improved treatment outcomes, including reducing side effects in chemotherapy.

Keywords

Inhalation therapy; Aerosols; Lungs; SPION; Magnetic; *In vitro* airways

*Corresponding author. sznitman@bm.technion.ac.il (J. Sznitman).

Declaration of Competing Interest

The authors declare that they have no known competing financial interests or personal relationships that could have appeared to influence the work reported in this paper.

Europe PMC Funders Author Manuscripts

1 Introduction

Inhalation aerosols are a hallmark of respiratory therapy, yet the ability to target either a specific pulmonary region (e.g. lung lobe) or a localized spot in the airway tree (e.g. tumors in bronchogenic carcinoma) remains generally poor (Heller-Algazi et al., 2020; Ostrovski et al., 2018; Stein and Thiel, 2017). Such drawback leads for example to higher risks of side effects and lower bioavailabilty (Velkov et al., 2014); a point particularly relevant in lung cancer (Stewart and Wild, 2014; Zarogoulidis et al., 2012a). Namely, one of the significant shortcomings of systemic chemotherapy lies in low doses of therapeutics that reach cancerous cells, with typical uptakes of ~ 1% in the entire lungs (Van Der Veldt et al., 2010). To overcome some of these challenges, topical delivery of chemotherapy via aerosol inhalation has been explored in preclinical animal (Gagnadoux et al., 2008; Garbuzenko et al., 2014; Gill et al., 2011; Hasenpusch et al., 2011; Hershey et al., 1999; Khanna and Vail, 2003; Konstantina et al., 2012; Mangal et al., 2017; Sharma et al., 2001; Yu et al., 2010; Zarogoulidis et al., 2012a) and clinical studies (Gagnadoux et al., 2008; Konstantina et al., 2012; Lemarie et al., 2011; Mangal et al., 2017; Otterson et al., 2010; 2007; 2013b;; Sharma et al., 2001; Tatsumura et al., 1993; Verschraegen et al., 2004; Zarogoulidis et al., 2013a), with a number of pertinent reviews available (Gagnadoux et al., 2008; Khanna and Vail, 2003; Konstantina et al., 2012; Mangal et al., 2017; Minko et al., 2013; Rosière et al., 2019; Sharma et al., 2001; Zarogoulidis et al., 2013a; 2012a). Outcomes of clinical trials (Rosière et al., 2019) have shown promising results, including reduced systemic side effects (Lemarie et al., 2011; Otterson et al., 2010, 2007; Tatsumura et al., 1993), tolerable adverse effects in healthy pulmonary tissue (Lemarie et al., 2011; Otterson et al., 2010, 2007; Tatsumura et al., 1993; Zarogoulidis et al., 2012b) and survival increase in phase II trials (Otterson et al., 2010; Zarogoulidis et al., 2012b). Nevertheless, several hurdles have hampered the wider use of inhaled chemotherapies, as lung toxicities still pose a real challenge (Mangal et al., 2017), and large quantities of drugs are lost in the surrounding environment with common inhalers or deposit in undesired lung locations (Ostrovski et al., 2016; Zarogoulidis et al., 2012a).

It has been hypothesized that some of these drawbacks could be alleviated through the incorporation of magnetic agents into the inhalable drugs and thereby control lung deposition using external magnetic fields (Christian, 2008; Longest and Holbrook, 2012; Saadat et al., 2020); a concept that has been extensively explored *in silico* over the past decade with computational fluid dynamic simulations (Kenjereš and Tjin, 2017; Manshadi et al., 2019; Martinez et al., 2012; Pourmehran et al., 2015). Since the aerodynamic drag forces exerted on airborne inhaled particles are vastly stronger than the magnetic force imposed by magnets, deflecting particles under airflow and depositing them on target has been limited. For example, in an *in vitro* study supported by numerical simulations Xie et al. (Xie et al., 2010a; 2010b) used aerosols of various SPION (superparamagnetic iron oxide nanoparticles) concentrations directed through glass tubes in the presence of a permanent magnet where increasing inhalation flow rates resulted in decreased deposition, as the magnet had less time to pull particles towards the wall.

Perhaps the most promising results have come from preclinical *in vivo* animal studies. The seminal work of Dames *et al.* (Dames et al., 2007) in rodents demonstrated a local increase in lung deposition in the presence of a magnet; 3.5 μm droplets were nebulized with 3.5%

v/v of SPIONs, leading to a 2.5 fold increase in deposition in the lung exposed to the magnetic field compared with the other lung. In their footsteps, a number of preclinical *in vivo* studies have further supported the idea of augmented deposition of magnetic particles at a local level (e.g. lung lobe), using both dry powders and nebulized suspensions (Hasenpusch et al., 2012; Price et al., 2017; Redman et al., 2011; Xie et al., 2010a). From a toxicity standpoint, SPIONs have been in clinical use as imaging contrast agents for many years (Bellin, 2006; Saito et al., 2005) and can be combined with various therapeutics (Dames et al., 2007; Poh et al., 2019) (e.g. chemotherapy, antibiotics).

Despite such progress, the ability to locally target aerosol deposition at a selected airway site while avoiding undesired deposition across the broader respiratory tract has faced several technical challenges. Namely, in addition to the previously mentioned role of drag forces on airborne particles, two concurrently limiting factors have hampered the targeting efficiency (i.e. the *deposition ratio* between the number of particles depositing in the targeted region to the untargeted), yielding a factor of two or three at best (Dames et al., 2007; Price et al., 2017). First, the magnetic field arising in the vicinity of the external magnet is always stronger than that further away from it. This characteristic has curtailed efficient targeting of specific airway sites due to deposition in the airway space between the target and the magnet. In parallel, most commonly-inhaled aerosolized medicines (i.e. typically ~ 1–5 μm diameter (Laube, 2005; Stein and Thiel, 2016)) are specifically intended to increase deposition along the respiratory tract. Hence, high particle deposition fractions of common inhalation aerosols limit the selective targeting ability due to broad airway deposition as a result of other physical determinants for such particle size range, most notably the role of sedimentation (Koullapis et al., 2018; Sznitman, 2013).

Motivated by these shortcomings, we present in an *in vitro* proof-of concept an inhalation framework to locally target a selected site in reconstructed airway models. The general delivery method revolves around a smart inhaler coupled with a ventilation machine and an external magnet. To minimize magnetic deposition of airborne particles located in the airspace between the magnet and the target airway site, the inhaler generates a short pulsed bolus of SPION-laden aerosolized droplets, after which the ventilator tracks the volume of air pushed behind the bolus to reach the targeted site along the airway path. Unlike traditional inhalation approaches, we confine aerosols to a tight bolus rather than a continuous stream, thereby minimizing airborne particles located in the airways between the magnet and the target; this approach drastically reduces undesired deposition in untargeted regions. Subsequently, we implement a short breath-hold maneuver that momentarily annuls the drag forces induced during airflow and thus increases significantly the magnet's ability to augment deposition. Importantly, our inhaler delivers aerosols in the submicron size range (~500 nm) that are overwhelmingly exhaled under normal breathing due to weak diffusional and gravitational forces (Hofemeier et al., 2018; Hofemeier and Sznitman, 2015; Sznitman, 2013); such particles are widely considered a poor choice in traditional inhalation therapy (Stahlhofen et al., 1989). Here, we leverage this characteristic to increase the deposition ratio several folds whereby aerosols located away from the magnetic field remain airborne throughout the inhalation protocol, and are thereafter exhaled.

2 Methods

The *in vitro* setup is schematically presented in Fig. 1 and combines a (i) custom-built smart inhaler that releases a short controlled pulse of SPION-loaded nebulized aerosols, through the ventilator-nebulizer junction (VNJ) connected via an endotracheal intubation tube (EIT) into the airway model (Fig. 2). (ii) In parallel, the custom-built ventilation machine controls and tracks the volume of air pushed into the model airways behind the aerosol bolus until the selected airway depth. (iii) Upon reaching the target volume, the ventilator momentarily halts with a short breath hold (BH). During BH, (iv) the permanent magnet assembly positioned near the targeted airway quickly draws the inhaled aerosols to deposit. Finally, (v) the cycle continues with ventilation reversal, thereby exhaling the remaining airborne particles from untargeted regions out of the model's trachea. Details on the ventilation machine and smart inhaler design are provided in the Appendix.

2.1 In vitro upper airway models

To first model a main bronchial bifurcation, we 3d print (Form 2 printer with Clear resin, Formlabs) a carinal bifurcation that connects a 16.8 mm tracheal glass tube to two 12.65 mm bronchi-mimicking glass tubes; the model follows representative morphometric measurements in a human adult lung (Heller-Algazi et al., 2020; Ostrovski et al., 2018). The magnet is placed next to one bronchus (see Results & Discussion); experiments are filmed from above illuminated by a continuous wave laser sheet (diode pumped solid state, 532 nm wavelength, 2.26 W, LaVision GmbH). We place a rolled transparency film in each of the bronchi to capture deposited aerosols ahead of quantification (see below). We use an off-the-shelf assembly of cylindrical permanent rare earth magnets, placed vertically, adjacent and perpendicular to the glass tube (i.e. four disc-shaped magnet 30 mm in diameter, 15 mm in height, separated by 5 mm thick plastic plates); the magnetic field at the surface of the magnet is measured at 0.35–0.4 T. We calibrate the BH initiation time to stop the pulse directly beneath the magnet for 5 s, which allows aerosols sufficient time to migrate towards the tube wall.

To quantify deposition we add fluorescent particles to the nebulized solution, with a 0.5 ml fluorescent bead solution (0.52 μm fluorescent red fluorescent polymer microspheres, 1% solids in DI water V/V, Fluoro-Max, Thermo Scientific), 0.5 ml DI water and 1 ml SPION solution (EMG 700 ferrofluid, Ferrotec); i.e. the final composition is 96.85% DI water, 2.9% SPIONs, 0.25% fluorescent particles. We run experiments until the entire 2 ml of solution is aerosolized, resulting in ~ 70 repeated aerosol boluses. We insert a rolled transparency film into the glass tube to serve as bedding for particle deposition and fluorescent particle count. Following the experiment, the transparency film is removed, flattened, and imaged (Zyla sCMOS, Andor) under fluorescent microscopy (Eclipse Ti, Nikon). Particle deposition locations are mapped, allowing to extract deposition density maps down to a single particle resolution. To ensure that data analysis is consistent, a known dilution of the fluorescent fluid was first tested (1:50,000), where results are found to match the fluorescent particle solution datasheet.

Next, we explore focused targeting in a four-generation airway model (i.e. corresponding to the first four generations of a 3D upper airway model recently introduced in *in silico*

studies (Heller-Algazi et al., 2020; Ostrovski et al., 2018)). To quantify deposition, we 3d print the airway tree as two halves (Fig. 3). To create a bedding for particle deposition we cover each half with a paraffin film (Parafilm, Bemis), and heat it with a blower at 150 °C, causing the film to soften and marry the model shape. The two model halves are then tightly closed. Rotameters (LZB-3WB 40–400 ml, Chinwey) are connected to each of the four exits of the model, and flow rates are tuned according to physiological measurements (Asgharian and Price, 2006; Walenga et al., 2013; Yin et al., 2010) using the rotameter valves, in conjunction with a more accurate digital flowmeter (Mass Flowmeter 4140, TSI). Finally, the model is positioned horizontally (similar to a patient laying on their back), while the magnet is positioned vertically above the model (see Results & Discussion). Following exposure of a 2 ml magnetic and fluorescent solution, the two halves of the model are separated and the Parafilm of each half is cut into slices (see Results & Discussion). Each slice is then washed in 1 ml of DI water for 60 s using a vortex shaker. Droplets of 1 μl are dripped onto microscope glass slides and left to evaporate at room temperature, leaving fluorescent and magnetic particles as residue. We count under fluorescent microscopy (see above) the fluorescent beads in each droplet's residue, to quantify the deposition on the examined Parafilm slices.

3 Results & discussion

3.1 Characterization of the pulsed aerosol bolus size distribution

Following established protocols for inhalation aerosols (De Boer et al., 2002), we first measured the size distribution of the nebulized aerosols generated from the smart inhaler using laser diffraction analysis (Spraytec, Malvern Panalytical Ltd.) and characterized the ensuing mean mass median aerodynamic diameter (MMAD). Results (i.e. mean and standard deviations) are presented following continuous 2 min measurements (with an acquisition rate of 1 Hz). We first report the size distribution measured at the outlet of the jet-nebulizer cup for a brine solution, i.e. DI water + NaCl 10:1 w/w solution. As anticipated (Fig. 4a), a large portion of the mass of the particles lies in the typical inhalable particle range (1–10 μm) with a MMAD of 4.41 ± 0.68 μm. Correspondingly, the aerosol size distribution for the smart inhaler has a MMAD of 0.45 ± 0.03 μm (Fig. 4b) for the SPION-laden solution (2.9% v/v SPION in DI water). We note that >90% of the aerosol mass is contained in aerosols of diameters < 1 μm (d_{90} = 0.961 ± 0.0610 μm). As the pulsed aerosol bolus travels through tubing and valves of the smart inhaler, this dead space acts as screen such that larger particles are likely to be filtered leaving the resulting distribution closer to the optimal range initially sought (~300–550 nm). To ensure that the presence of SPIONs does not cause a significant distortion in the particle size measurements we compared results for the SPION suspension to the brine solution yielding a similar distribution, with an MMAD of 0.501 ± 0.0177 μm and d_{90} = 1.17 ± 0.03 μm (distribution not shown here for brevity).

3.2 Magnetic aerosol targeting in bifurcating in vitro airways

We explore localized targeting in a simple bifurcating airway structure, a case study representing the two first bronchi past the trachea of representative adult-sized airways. We arbitrarily select to target one of the two daughter bifurcations by placing the magnet

assembly near the external wall of the tube (Fig. 5a). Upon inhalation, the pulsed aerosol bolus divides into each daughter airway and particles are pulled towards the magnet in the targeted bronchus, while remaining airborne in the untargeted branch prior to exhalation (Fig. 5a; see SM Video 1). We quantify (following 70 repeated pulsed boli) the resulting deposition pattern underlining the bolus shape on the airway lumen, and observe a deposition hot spot located downstream near the head of the bolus with a more dilute pattern around the bolus tail (Fig. 5b). We note the presence of a small concentration of deposited particles outside the target region near the carina (Fig. 5b; see bottom right corner of the tube), but remarkably no particles are identified in the untargeted branch. Quantitatively, our results yield 98.8% of the particles deposit in the targeted region under the magnet; this would correspond to an ideal 80.5 targeting ratio (i.e. notwithstanding exhaled particles that do not deposit). While this simple configuration is limited in the possibilities for superfluous deposition arising in a single bifurcation, it is nevertheless relevant in the context of targeting localized tracheobronchial tumors in the regions of the trachea and main bronchi (Ma et al., 2018; Stevic and Milenkovic, 2016).

Multimedia Component 1 Video 1 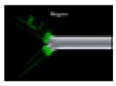 https://pcv3-elsevier-live.s3.amazonaws.com/ba88a7f36d33c65d53599c2e0866a4/image/mmc1.mp4

A broader question in assessing our inhalation framework lies in whether the BH maneuver itself (i.e. after reaching the target airway depth) is necessary in order to achieve localized targeting. To address this issue, we ran an experiment with no BH using a simple glass tube with a diameter corresponding to a representative average adult human trachea (16.5 mm), as motivated by recent *in silico* (Pourmehran et al., 2015) *and in vitro* studies (Poh et al., 2019). Even at the low flow rate implemented in our experiment (i.e. 1.145 l/min), the magnet assembly could merely cause a small deflection to the aerosol pulse (Fig. 6; compare SM video 2 and 3), underlining the role of aerodynamic drag forces on airborne particles during flight (Heller-Algazi et al., 2020; Ostrovski et al., 2018; 2016). A parallel question lies in whether once the bolus is stopped above the targeted location, would it be possible to allow the particles to sediment under gravity, circumventing the need of a magnet altogether. We found that for the given particle size distribution of the smart inhaler (Fig. 4b) sedimentation occurs on the order of several minutes (not shown here for brevity); an unrealistic time frame for a clinical BH maneuver that is in line with advocating the use of micron-sized aerosols in common inhalation therapy (Stahlhofen et al., 1989; Stein and Thiel, 2017).

Multimedia Component 2 Video 2 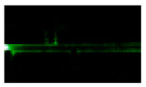 https://pcv3-elsevier-live.s3.amazonaws.com/ba88a7f36d33c65d53599c2e0866a4/image/mmc1.mp4

Multimedia Component 3 Video 3 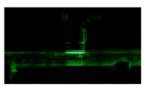 https://pcv3-elsevier-live.s3.amazonaws.com/ba88a7f36d33c65d53599c2e0866a4/image/mmc1.mp4

In a next step, we demonstrate magnetic focused targeting in a more physiologically-realistic human airway geometry spanning several asymmetric generations (see Methods). In the present proof-of-concept, we arbitrarily select a target site located in an airway past the second generation of the left lung; here, we present results upon successive repeats (n = 70) of targeted boli at the selected site to exemplify the repeatability of the technique. Consistent results lead to a black stain of SPI-ONs visible under the magnet in Fig. 7a. Deposition results (Fig. 7b) are extracted according to the slice area (i.e. particles per unit area, or PPA in $1/mm^2$) and normalized by the maximum measured PPA value. We observe significant differences as the relative deposition density in the region under the magnet is >10 times larger compared to the next highest value elsewhere in the airway model. Values of 1 ± 0.22 and 0.59 ± 0.19 are retrieved in the red and yellow regions under the magnet, respectively; a value of 0.09 ± 0.03 is found in the left bronchus in the bottom airway half. Some remaining superfluous deposition is seen in the top half of the model, i.e. in the branches that are at the same distance from the model inlet as the targeted region. By and large, the *in vitro* targeting ability of the method underlines repeatability and precision with strong potential for significantly augmenting the aerosol targeting efficiency.

3.3 From proof-of-concept to clinical applications

We discuss some of the limitations of the inhalation framework presented, leaving aside discussions relating to the safety and efficacy of its therapeutic potential. In the current setup, *in vitro* experiments correspond closest to a scenario whereby a patient is intubated and mechanically ventilated. While the endotracheal intubation of the model circumvents the occurrence of aerosol dispersion phenomena due to the laryngeal jet (Das et al., 2018; Heller-Algazi et al., 2020), our first embodiment holds clinical applications in specialized inhalation therapies (Fink and Ari, 2013). With this in mind, voluntary oral inhalation through an inhaler device would significantly broaden the applicability of the technique. Although beyond the present scope, this could be realized by requesting for instance the patient to breathe through the device and comply with the prescribed flow or alternatively by monitoring voluntarily inhaled volumes using a spirometer. We note that while our method relies on prior knowledge of the targeted airway site (i.e. via the tracked volume of air pushed behind the aerosol bolus), our approach is first motivated by patients who have previously undergone imaging diagnostics (e.g. computed tomography) to identify and localize the presence of a malignant tumor (de Jong et al., 2005; Park et al., 2009).

Our experiments are confined to a permanent magnet assembly in close vicinity to the targeted airway. While the magnetic fields imposed here are relatively elevated in such proximity with the focused targeting point, magnetic fields decrease rapidly with increasing distance from the magnet; a point to consider in clinical applications as the external magnet should be placed near a patient's cavity chest but still potentially distant from a targeted airway (i.e. mm to cm). Although the construction of such magnet is outside the present scope, we consider some existing designs in view of the clinical feasibility of implementing our proof-of-concept; a more thorough overview of such magnetic systems are discussed elsewhere (Cao et al., 2011; Saadat et al., 2020; Shapiro et al., 2015). For example, Alexiou *et al.* (Alexiou et al., 2006) constructed a hybrid system for magnetic (cardiovascular) drug targeting, where electromagnetic coils were wrapped around a permanent magnet core.

Although their system was relatively small, the authors underline its scalability. Takeda *et al.* (Takeda et al., 2006) developed magnetic particles for gene transfer using viral vectors, and established the feasibility of such system to facilitate targeted particle delivery. Following (Alexiou et al., 2006), Gleich *et al.* (Gleich et al., 2007) developed a larger magnet based on a similar design, where two parallel coils with 2000 loops were each wrapped around iron-cobalt alloy cores, that were cone-shaped to increase magnetic field gradients; their system was designed for vascular targeting in preclinical *in vivo* experiments in pigs, and with a 20 cm distance between the magnets such setup could be adapted for the present targeted inhalation framework.

4 Conclusions

In an *in vitro* proof-of-concept, we have presented a targeted inhalation framework revolving around a smart inhaler that releases a short pulse of SPION-laden nebulized aerosols coupled with a ventilation machine that controls the volume of air pushed into the airway geometry model, thus tracking the location of the bolus. The ventilator then momentarily halts, leading to a short breath-hold maneuver. A magnet positioned near the targeted airway site quickly draws the aerosols in its vicinity, forcing them to quickly deposit during breath hold. The cycle continues with the reversal of the ventilator, thus exhaling the remaining airborne particles from depositing in untargeted regions. Deposition within the vicinity of the magnet is quantified via fluorescence microscopy and we observe *in vitro* a ten-fold higher particle deposition density in the targeted region compared to the highest density elsewhere in the 3d printed reconstructed upper airway model. Such magnetic inhalation targeting strategy may pave the way for improved treatment outcomes and reduced side effects in specialized inhalation therapies, including chemotherapy.

Acknowledgement

This work was supported by the European Research Council (ERC) under the European Union's Horizon 2020 research and innovation program (grant agreement No 677772) and the Kamin Fund (grant no. 60509) by the Israel Innovation Authority. We kindly thank financial support from the Technion (Star Foundation).

References

Alexiou C, Diehl D, Henninger P, Iro H, Rockelein R, Schmidt W, Weber H. A high field gradient magnet for magnetic drug targeting. IEEE Trans Appl Supercond. 2006; 16 :1527–1530. DOI: 10.1109/TASC.2005.864457

Asgharian B, Price O. Airflow distribution in the human lung and its influence on particle deposition. Inhal Toxicol. 2006; 18 :795–801. DOI: 10.1080/08958370600748687 [PubMed: 16774869]

Bellin M-F. MR contrast agents, the old and the new. Eur J Radiol. 2006; 60 :314–323. DOI: 10.1016/j.ejrad.2006.06.021 [PubMed: 17005349]

Cao Q, Han X, Li L. Enhancement of the efficiency of magnetic targeting for drug delivery: development and evaluation of magnet system. J Magn Magn Mater. 2011; 323 :1919–1924. DOI: 10.1016/j.jmmm.2010.11.058

Christian P. Nanomagnetosols: magnetism opens up new prespectives for targeted aerosol delivery to the lung. Trends Biotechnol. 2008; 26 :59–63. DOI: 10.1016/j.tibtech.2007.10.010 [PubMed: 18191261]

Dames P, Gleich B, Flemmer A, Hajek K, Seidl N, Wiekhorst F, Eberbeck D, Bittmann I, Bergemann C, Weyh T, Trahms L, et al. Targeted delivery of magnetic aerosol droplets to the lung. Nat Nanotechnol. 2007; 2 :495–499. DOI: 10.1038/nnano.2007.217 [PubMed: 18654347]

Das P, Nof E, Amirav I, Kassinos SC, Sznitman J. Targeting inhaled aerosol delivery to upper airways in children: Insight from computational fluid dynamics (CFD). PLoS ONE. 2018; 13 :1–20. DOI: 10.1371/journal.pone.0207711

De Boer AH, Gjaltema D, Hagedoorn P, Frijlink HW. Characterization of inhalation aerosols: a critical evaluation of cascade impactor analysis and laser diffraction technique. Int J Pharm. 2002; 249 :219–231. DOI: 10.1016/S0378-5173(02)00526-4 [PubMed: 12433450]

de Jong PA, Mueller NL, Pare PD, Coxson HO. Computed tomographic imaging of the airways: relationship to structure and function. Eur Respir J. 2005; 26 :140–152. DOI: 10.1183/09031936.05.00007105 [PubMed: 15994401]

Fink J, Ari A. Aerosol delivery to intubated patients. Expert Opin Drug Deliv. 2013; 10 :1077–1093. DOI: 10.1517/17425247.2013.790362 [PubMed: 23614495]

Gagnadoux F, Hureaux J, Vecellio L, Urban T, Le Pape A, Valo I, Montharu J, Leblond V, Boisdron-Celle M, Lerondel S, Majoral C, et al. Aerosolized chemotherapy. J Aerosol Med Pulm Drug Deliv. 2008; 21 :61–70. DOI: 10.1089/jamp.2007.0656 [PubMed: 18518832]

Garbuzenko OB, Mainelis G, Taratula O, Minko T. Inhalation treatment of lung cancer: the influence of composition, size and shape of nanocarriers on their lung accumulation and retention. Can Biol Med. 2014; 11 :44–55. DOI: 10.7497/j.issn.2095-3941.2014.01.004

Gill KK, Nazzal S, Kaddoumi A. Paclitaxel loaded PEG5000-DSPE micelles as pulmonary delivery platform: formulation characterization, tissue distribution, plasma pharmacokinetics, and toxicological evaluation. Eur J Pharm Biopharm. 2011; 79 :276–284. DOI: 10.1016/j.ejpb.2011.04.017 [PubMed: 21575719]

Gleich B, Hellwig N, Bridell H, Jurgons R, Seliger C, Alexiou C, Wolf B, Weyh T. Design and evaluation of magnetic fields for nanoparticle drug targeting in cancer. IEEE Trans Nanotechnol. 2007; 6 :164–169. DOI: 10.1109/TNANO.2007.891829

Hasenpusch G, Geiger J, Wagner K, Mykhaylyk O, Wiekhorst F, Trahms L, Heidsieck A, Gleich B, Bergemann C, Aneja MK, Rudolph C. Magnetized aerosols comprising superparamagnetic iron oxide nanoparticles improve targeted drug and gene delivery to the lung. Pharm Res. 2012; 29 :1308–1318. DOI: 10.1007/s11095-012-0682-z [PubMed: 22271050]

Hasenpusch G, Pfeifer C, Aneja MK, Wagner K, Reinhardt D, Gilon M, Ohana P, Hochberg A, Rudolph C. Aerosolized bc-819 inhibits primary but not secondary lung cancer growth. PLoS ONE. 2011; 6 doi: 10.1371/journal.pone.0020760

Heller-Algazi M, Nof E, Das P, Bhardwaj S, Kassinos SC, Sznitman J. In silico optimization of targeted aerosol delivery in upper airways via inhaled volume tracking. Clin Biomech. 2020; 80 105138 doi: 10.1016/j.clinbiomech.2020.105138

Hershey AE, Kurzman ID, Forrest LJ, Bohling CA, Stonerook M, Placke ME, Imondi AR, Vail DM. Inhalation chemotherapy for macroscopic primary or metastatic lung tumors: proof of principle using dogs with spontaneously occurring tumors as a model. Clin Cancer Res. 1999; 5 :2653–2659. [PubMed: 10499645]

Hofemeier P, Koshiyama K, Wada S, Sznitman J. One (sub-)acinus for all: fate of inhaled aerosols in heterogeneous pulmonary acinar structures. Eur J Pharm Sci. 2018; 113 :53–63. DOI: 10.1016/j.ejps.2017.09.033 [PubMed: 28954217]

Hofemeier P, Sznitman J. Revisiting pulmonary acinar particle transport: convection, sedimentation, diffusion and their interplay. J Appl Physiol. 2015; jap.01117.2014 doi: 10.1152/japplphysiol.01117.2014

Kenjereš S, Tjin JL. Numerical simulations of targeted delivery of magnetic drug aerosols in the human upper and central respiratory system: a validation study. R Soc Open Sci. 2017; 4 170873 doi: 10.1098/rsos.170873 [PubMed: 29308230]

Khanna C, Vail DM. Targeting the lung: preclinical and comparative evaluation of anticancer aerosols in dogs with naturally occurring cancers. Curr Can Drug Targets. 2003; 3 :265–273. DOI: 10.2174/1568009033481903

Konstantina S, Eirini C, Panos M. Medication for the treatment of lung cancer. 2012; 1 :298.

Koullapis PG, Hofemeier P, Sznitman J, Kassinos SC. An efficient computational fluid-particle dynamics method to predict deposition in a simplified approximation of the deep lung. Eur J Pharm Sci. 2018; 113 :132–144. DOI: 10.1016/j.ejps.2017.09.016 [PubMed: 28917963]

Laube BL. The expanding role of aerosols in systemic drug delivery, gene therapy, and vaccination. Respir Care. 2005; 50 :1161–1176. DOI: 10.1186/2213-0802-2-3 [PubMed: 16122400]

Lemarie E, Vecellio L, Hureaux J, Prunier C, Valat C, Grimbert D, Boidron-Celle M, Giraudeau B, le Pape A, Pichon E, Diot P, et al. Aerosolized gemcitabine in patients with carcinoma of the lung: feasibility and safety study. J Aerosol Med Pulm Drug Deliv. 2011; 24 :261–270. DOI: 10.1089/jamp.2010.0872 [PubMed: 21793717]

Longest PW, Holbrook LT. In silico models of aerosol delivery to the respiratory tract — development and applications. Adv Drug Deliv Rev. 2012; 64 :296–311. DOI: 10.1016/j.addr.2011.05.009 [PubMed: 21640772]

Ma K, Sun F, Yang X, Wang S, Wang L, Jin Y, Shi Y, Jiang W, Zhan C, Wang Q. Prognosis of patients with primary malignant main stem bronchial tumors: 7418 cases based on the SEER database. Onco Targets Ther. 2018; 11 :83–95. DOI: 10.2147/OTT.S142847 [PubMed: 29317836]

Mangal S, Gao W, Li T, Zhou QT. Pulmonary delivery of nanoparticle chemotherapy for the treatment of lung cancers: challenges and opportunities. Acta Pharmacol Sin. 2017; 38 :782–797. DOI: 10.1038/aps.2017.34 [PubMed: 28504252]

Manshadi MKD, Saadat M, Mohammadi M, Kamali R, Shamsi M, Naseh M, Sanati-Nezhad A. Magnetic aerosol drug targeting in lung cancer therapy using permanent magnet. Drug Deliv. 2019; 26 :120–128. DOI: 10.1080/10717544.2018.1561765 [PubMed: 30798633]

Martinez RC, Roshchenko a, Minev P, Finlay WH. Simulation of Enhanced Deposition Due to Magnetic Field Alignment of Ellipsoidal Particles in a Lung Bifurcation. J Aerosol Med Pulm Drug Deliv. 2012; 26 120502122821003 doi: 10.1089/jamp.2011.0921

Minko T, Rodriguez-Rodriguez L, Pozharov V. Nanotechnology approaches for personalized treatment of multidrug resistant cancers. Adv Drug Deliv Rev. 2013; 65 :1880–1895. DOI: 10.1016/j.addr.2013.09.017 [PubMed: 24120655]

Ostrovski Y, Dorfman S, Mezhericher M, Kassinos S, Sznitman J. Targeted drug delivery to upper airways using a pulsed aerosol bolus and inhaled volume tracking method. Flow Turbul Combust. 2018; :1–15. DOI: 10.1007/s10494-018-9927-1

Ostrovski Y, Hofemeier P, Sznitman J. Augmenting regional and targeted delivery in the pulmonary acinus using magnetic particles. Int J Nanomedicine. 2016; 11 :3385–3395. DOI: 10.2147/IJN.S102138 [PubMed: 27547034]

Otterson GA, Villalona-Calero MA, Hicks W, Pan X, Ellerton JA, Gettinger SN, Murren JR. Phase I/II study of inhaled doxorubicin combined with platinum-based therapy for advanced non-small cell lung cancer. Clin Can Res. 2010; 16 :2466–2473. DOI: 10.1158/1078-0432.CCR-09-3015

Otterson GA, Villalona-Calero MA, Sharma S, Kris MG, Imondi A, Gerber M, White DA, Ratain MJ, Schiller JH, Sandler A, Kraut M, et al. Phase I study of inhaled doxorubicin for patients with metastatic tumors to the lungs. Clin Can Res. 2007; 13 :1246–1252. DOI: 10.1158/1078-0432.CCR-06-1096

Park CM, Goo JM, Lee HJ, Min A. Tumors in the Tracheo- bronchial Tree : CT and. RadioGraphics. 2009; 29 :55–72. [PubMed: 19168836]

Poh W, AbRahman N, Ostrovski Y, Sznitman J, Pethe K, Loo SCJ. Active pulmonary targeting against tuberculosis (TB) via triple-encapsulation of Q203, bedaquiline and superparamagnetic iron oxides (SPIOs) in nanoparticle aggregates. Drug Deliv. 2019; 26 :1039–1048. DOI: 10.1080/10717544.2019.1676841 [PubMed: 31691600]

Pourmehran O, Rahimi-Gorji M, Gorji-Bandpy M, Gorji TB. Simulation of magnetic drug targeting through tracheobronchial airways in the presence of an external non-uniform magnetic field using Lagrangian magnetic particle tracking. J Magn Magn Mater. 2015; 393 :380–393. DOI: 10.1016/j.jmmm.2015.05.086

Price DN, Stromberg LR, Kunda NK, Muttil P. In vivo pulmonary delivery and magnetic-targeting of dry powder nano-in-microparticles. Mol Pharm. 2017; 14 :4741–4750. DOI: 10.1021/acs.molpharmaceut.7b00532 [PubMed: 29068693]

Redman GES, Martin AR, Waszak P, Thompson RB, Cheung P-Y, Thébaud B, Finlay WH. Pilot study of inhaled aerosols targeted via magnetic alignment of high aspect ratio particles in rabbits. J Nanomater. 2011; 2011 :1–7. DOI: 10.1155/2011/130721 [PubMed: 21808638]

Rosière R, Berghmans T, de Vuyst P, Amighi K, Wauthoz N. The position of inhaled chemotherapy in the care of patients with lung tumors: clinical feasibility and indications according to recent pharmaceutical progresses. Cancers (Basel). 2019; 11 doi: 10.3390/cancers11030329

Saadat M, Manshadi MKD, Mohammadi M, Zare MJ, Zarei M, Kamali R, Sanati-Nezhad A. Magnetic particle targeting for diagnosis and therapy of lung cancers. J Control Release. 2020; doi: 10.1016/j.jconrel.2020.09.017

Saito K, Shindo H, Ozuki T, Ishikawa A, Kotake F, Shimazaki Y, Abe K. Perfusion study of hypervascular hepatocellular carcinoma with SPIO. Magn Reson Med Sci. 2005; 4 :151–158. DOI: 10.2463/mrms.4.151 [PubMed: 16543699]

Shapiro B, Kulkarni S, Nacev A, Muro S, Stepanov PY, Weinberg IN. Open challenges in magnetic drug targeting. Wiley Interdiscip Rev Nanomedicine Nanobiotechnology. 2015; 7 :446–457. DOI: 10.1002/wnan.1311 [PubMed: 25377422]

Sharma S, White D, Imondi AR, Placke ME, Vail DM, Kris MG. Development of inhalational agents for oncologic use. J Clin Oncol. 2001; 19 :1839–1847. DOI: 10.1200/JCO.2001.19.6.1839 [PubMed: 11251016]

Stahlhofen W, Rudolf G, James aC. Intercomparison of Experimental Regional Aerosol Deposition Data. J Aerosol Med. 1989; 2 :285–308. DOI: 10.1089/jam.1989.2.285

Stein SW, Thiel CG. The history of therapeutic aerosols: a chronological review. J Aerosol Med Pulm Drug Deliv. 2017; 30 :20–41. DOI: 10.1089/jamp.2016.1297 [PubMed: 27748638]

Stein SW, Thiel CG. The history of therapeutic aerosols: a chronological review. J Aerosol Med Pulm Drug Deliv. 2016; 29 doi: 10.1089/jamp.2016.1297

Stevic R, Milenkovic B. Tracheobronchial tumors. J Thorac Dis. 2016; 8 :3401–3413. DOI: 10.21037/jtd.2016.11.24 [PubMed: 28066620]

Stewart, BW, Wild, CP. World cancer report 2014. World Health Organization; 2014.

Sznitman J. Respiratory microflows in the pulmonary acinus. J Biomech. 2013; 46 :284–298. DOI: 10.1016/j.jbiomech.2012.10.028 [PubMed: 23178038]

Takeda S-I, Mishima F, Terazono B, Izumi Y, Nishijima S. Development of magnetic force-assisted new gene transfer system using biopolymer-coated ferromagnetic nanoparticles. IEEE Trans Appl Supercond. 2006; 16 :1543–1546. DOI: 10.1109/TASC.2005.869695

Tatsumura T, Koyama S, Tsujimoto M, Kitagawa M, Kagamimori S. Further study of nebulisation chemotherapy, a new chemotherapeutic method in the treatment of lung carcinomas: fundamental and clinical. Br J Can. 1993; 68 :1146–1149. DOI: 10.1038/bjc.1993.495

Van Der Veldt AAM, Hendrikse NH, Smit EF, Mooijer MPJ, Rijnders AY, Gerritsen WR, Van Der Hoeven JJM, Windhorst AD, Lammertsma AA, Lubberink M. Biodistribution and radiation dosimetry of 11C-labelled docetaxel in cancer patients. Eur J Nucl Med Mol Imaging. 2010; 37 :1950–1958. DOI: 10.1007/s00259-010-1489-y [PubMed: 20508935]

Velkov T, Rahim NA, Zhou QT, Chan H-K, Li J. Inhaled anti-infective chemotherapy for respiratory tract infections: Successes, challenges and the road ahead. Adv Drug Deliv Rev. 2014; doi: 10.1016/j.addr.2014.11.004

Verschraegen CF, Gilbert BE, Loyer E, Huaringa A, Walsh G, Newman RA, Knight V. Clinical evaluation of the delivery and safety of aerosolized liposomal 9-nitro-20 (s) -Camptothecin in patients with advanced pulmonary malignancies. Clin Can Res. 2004; 10 :2319–2326. DOI: 10.1158/1078-0432.CCR-0929-3

Walenga RL, Tian G, Longest PW. Development of characteristic upper tracheobronchial airway models for testing pharmaceutical aerosol delivery. J Biomech Eng. 2013; 135 91010 doi: 10.1115/1.4024630 [PubMed: 23722698]

Xie Y, Longest PW, Xu YH, Wang JP, Wiedmann TS. In vitro and in vivo lung deposition of coated magnetic aerosol particles. J Pharm Sci. 2010a; 99 :4658–4668. DOI: 10.1002/jps.22168 [PubMed: 20845463]

Xie Y, Zeng P, Siegel Ra, Wiedmann TS, Hammer BE, Longest PW. Magnetic deposition of aerosols composed of aggregated superparamagnetic nanoparticles. Pharm Res. 2010b; 27 :855–865. DOI: 10.1007/s11095-010-0078-x [PubMed: 20198407]

Yin Y, Choi J, Hoffman Ea, Tawhai MH, Lin CL. Simulation of pulmonary air flow with a subject-specific boundary condition. J Biomech. 2010; 43 :2159–2163. DOI: 10.1016/j.jbiomech.2010.03.048 [PubMed: 20483412]

Yu K-N, Minai-Tehrani A, Chang S-H, Hwang S-K, Hong S-H, Kim J-HJ-E, Shin J-Y, Park S-J, Kim J-HJ-E, Kwon J-T, Jiang H-L, et al. Aerosol delivery of small hairpin osteopontin blocks pulmonary metastasis of breast cancer in mice. PLoS ONE. 2010; 5 e15623 doi: 10.1371/journal.pone.0015623 [PubMed: 21203518]

Zarogoulidis P, Chatzaki E, Porpodis K, Domvri K, Hohenforst-Schmidt W, Goldberg EP, Karamanos N, Zarogoulidis K. Inhaled chemotherapy in lung cancer: future concept of nanomedicine. Int J Nanomed. 2012a; 7 :1551–1572. DOI: 10.2147/IJN.S29997

Zarogoulidis P, Darwiche K, Kalamaras G, Huang H, Hohenforst-Schmidt W, Zarogoulidis K. Targeted versus chrono-targeted chemotherapy for inhaledchemotherapy in non-small cell lung cancer. Transl Lung Can Res. 2013a; 2 :E17–E22. DOI: 10.3978/j.issn.2218-6751.2012.12.07

Zarogoulidis P, Darwiche K, Krauss L, Huang H, Zachariadis GA, Katsavou A, Hohenforst-Schmidt W, Papaiwannou A, Vogl TJ, Freitag L, Stamatis G, et al. Inhaled cisplatin deposition and distribution in lymph nodes in stage II lung cancer patients. Futur Oncol. 2013b; 9 :1307–1313. DOI: 10.2217/fon.13.111

Zarogoulidis P, Eleftheriadou E, Sapardanis I, Zarogoulidou V, Lithoxopoulou H, Kontakiotis T, Karamanos N, Zachariadis G, Mabroudi M, Zisimopoulos A, Zarogoulidis K. Feasibility and effectiveness of inhaled carboplatin in NSCLC patients. Invest New Drugs. 2012b; 30 :1628–1640. DOI: 10.1007/s10637-011-9714-5 [PubMed: 21739158]

Europe PMC Funders Author Manuscripts

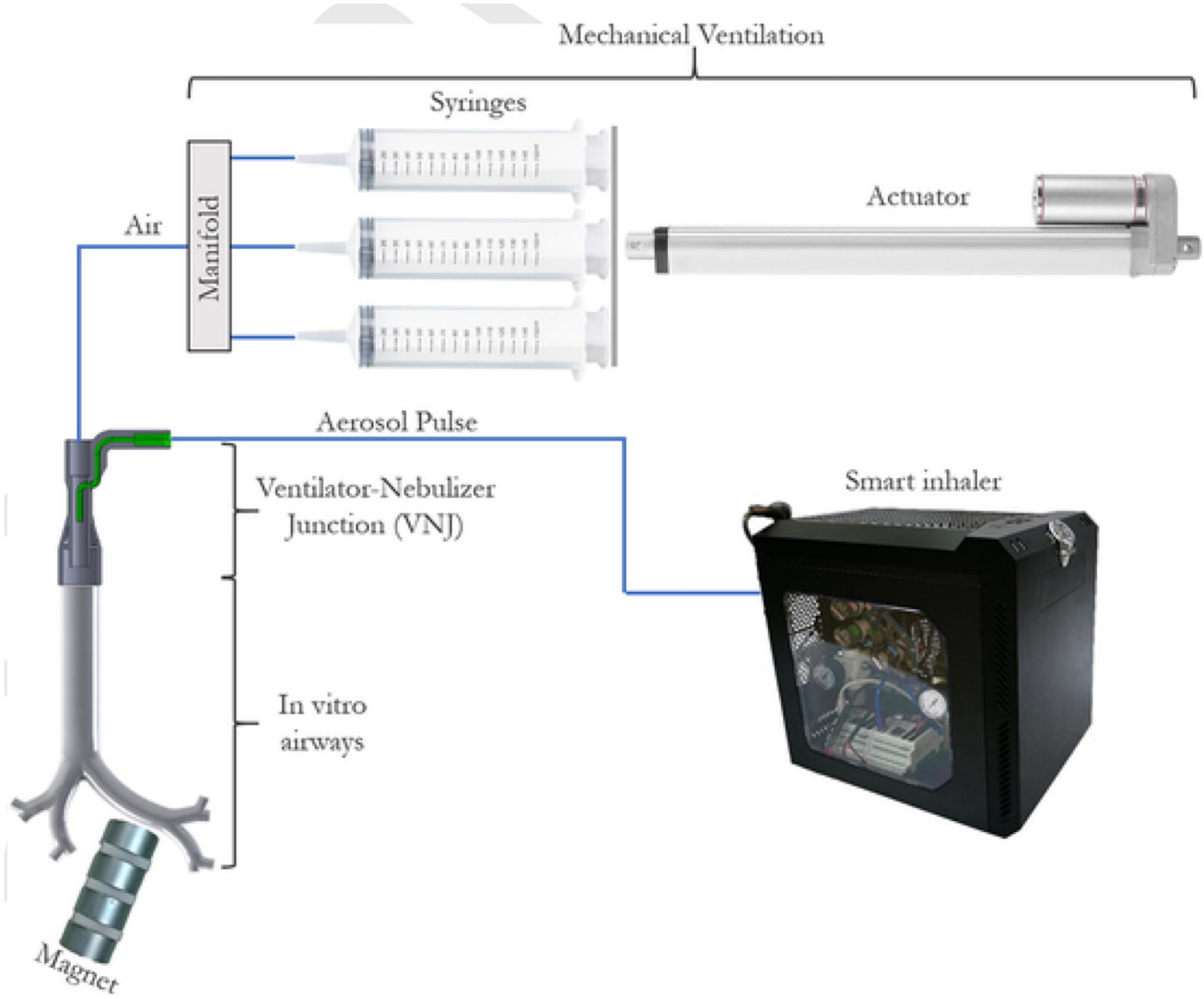

Fig. 1.

Schematic of the *in vitro* proof-of-concept setup for targeted aerosol delivery using magnetic particles and an external magnet. Briefly, a smart inhaler generates a short pulsed bolus of aerosolized SPION-laden droplets delivered via a ventilator-nebulizer junction (VNJ) into the airway model. The inhaler is connected to a custom-built mechanical ventilator and the entire system is electronically controlled (see Methods). Note that superfluous aerosols are pushed during the exhalation phase into the chemical hood through the manifold, via a tube parallel to the air line (not shown here for simplicity).

Europe PMC Funders Author Manuscripts

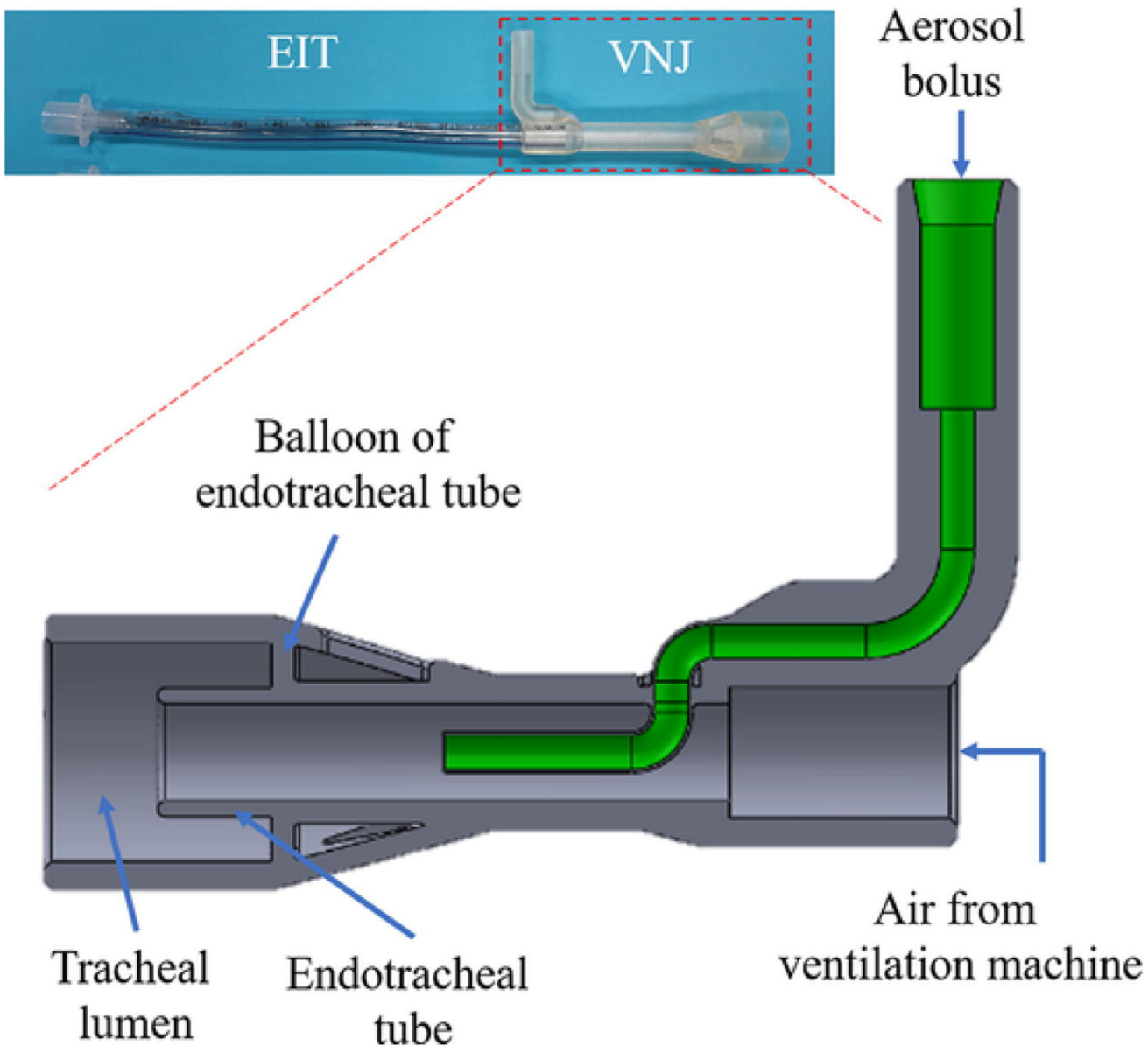

Fig. 2.

Schematic detail of the ventilator-nebulizer junction (VNJ) design and its assembly with an endotracheal intubation tube (EIT) to deliver the aerosol bolus into the trachea of the upper airway model.

Fig. 3. Snapshot of the two halves of the 3D printed multi-generation asymmetric upper airway model, coated with Parafilm.

Europe PMC Funders Author Manuscripts

Europe PMC Funders Author Manuscripts

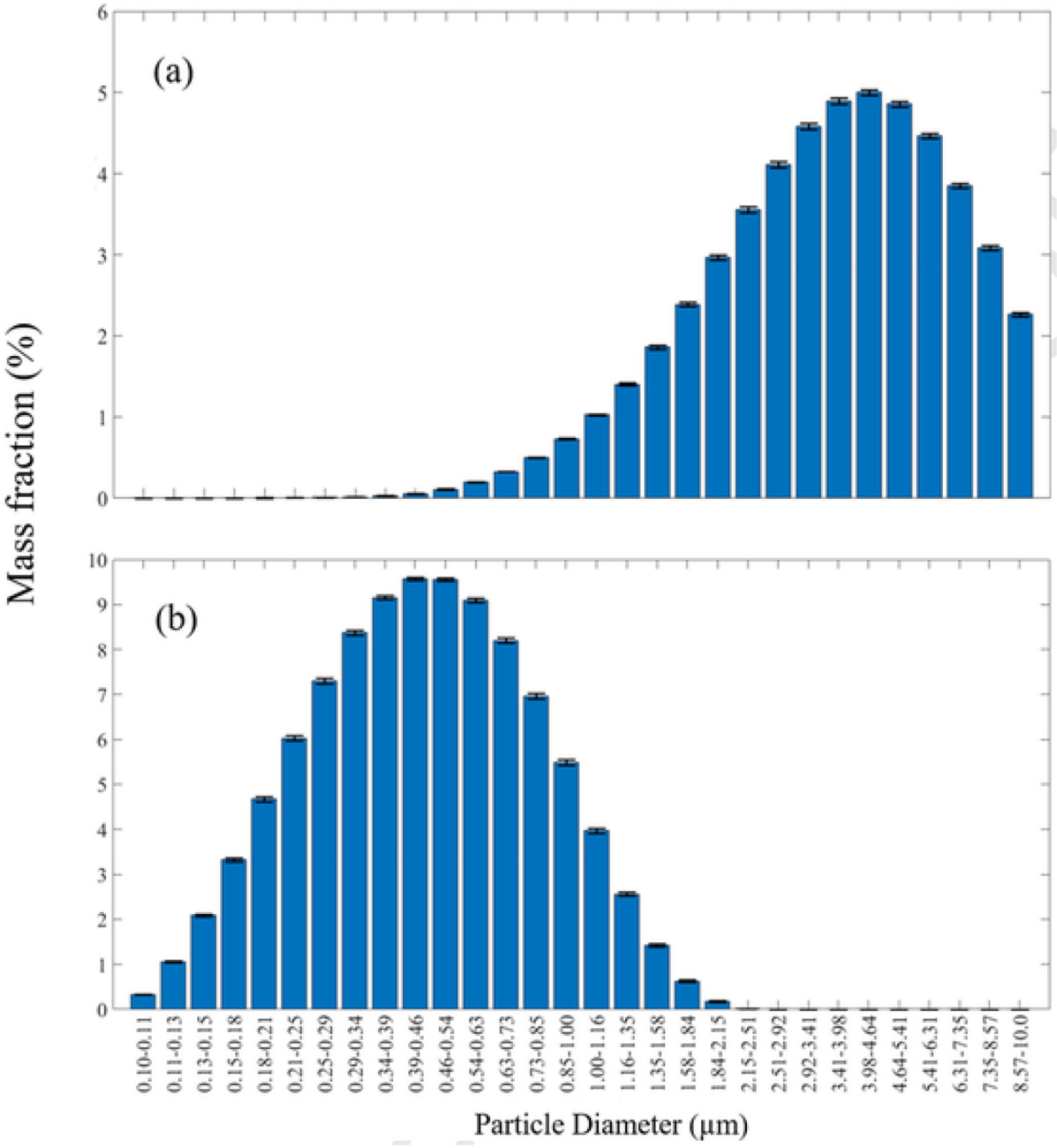

Fig. 4.

Distribution of the mass fraction according to particle diameter following laser diffraction analysis for (a) a brine solution exiting the commercial jet nebulizer cup (MMAD of 4.41 ± 0.68 µm) and (b) the SPION-loaded aerosol bolus exiting the smart inhaler (MMAD of 0.45 ± 0.03 µm).

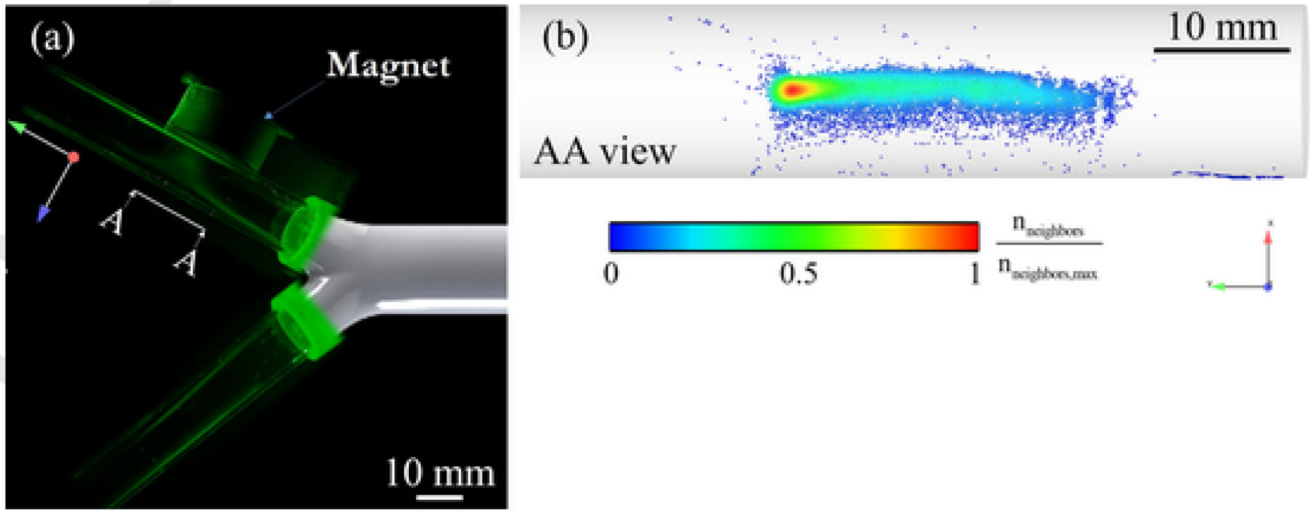

Fig. 5.

(a) Visualization of the aerosol bolus entering the two main bronchi of the bifurcating model, with the magnet placed in the vicinity of one bronchus. (b) Quantification of the relative deposition density of aerosols near the magnet (i.e. density map). Note that no particles were observed to reside elsewhere across the bifurcating airway model.

Europe PMC Funders Author Manuscripts

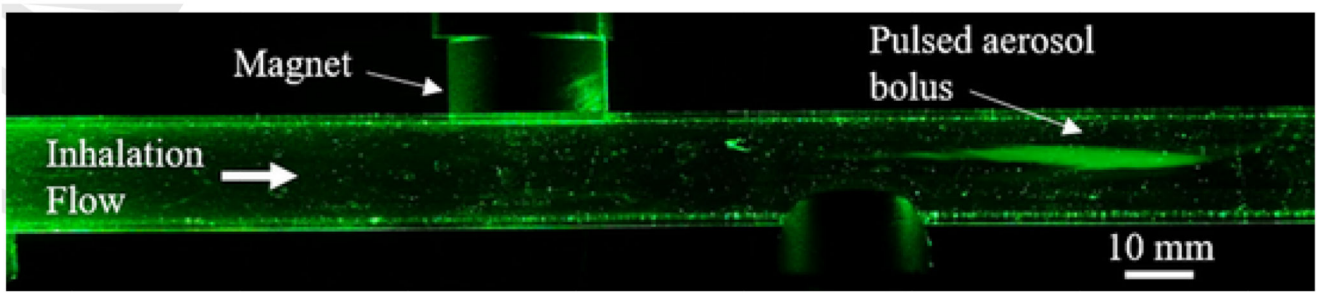

Fig. 6.

Instantaneous snapshot of a pulsed aerosol bolus traveling past the magnet in a glass tube (16.8 mm diameter) mimicking a human adult tracheal airway in the absence of a breath hold (BH) maneuver (at a fixed flow rate of 1.145 l/min). Even at low flow rate, the magnet cannot deflect the aerosol bolus and much less deposit the SPION-laden particles at the wall.

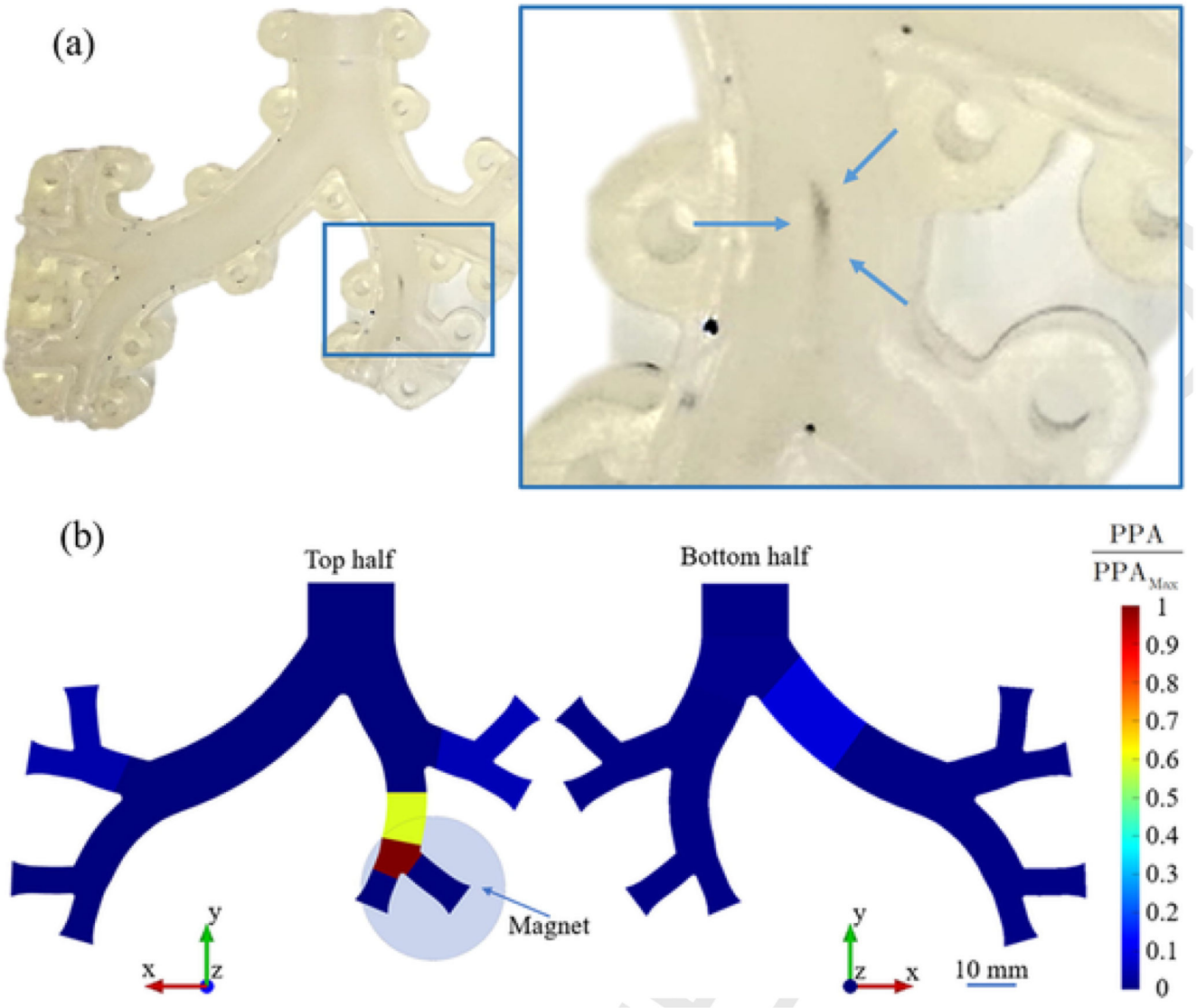

Fig. 7.

(a) Snapshot of the visible stain residue following repeated SPION-laden aerosol boli depositing consecutively in the near vicinity of the positioned magnet on the local airway (top half). (b) Corresponding deposition quantification of the normalized particles per area (PPA) according to the individual Parafilm slices prepared along the top and bottom halves of the 3D printed model (see Methods).